MOLECULAR AND CELLULAR BIOLOGY, Mar. 2008, p. 1702–1712 Vol. 28, No. 5
0270-7306/08/$08.00+0 doi:10.1128/MCB.01282-07

Mosaic Complementation Demonstrates a Regulatory Role for Myosin VIIa in Actin Dynamics of Stereocilia▽†

Haydn M. Prosser,[1]‡* Agnieszka K. Rzadzinska,[2]‡ Karen P. Steel,[2] and Allan Bradley[1]

Mouse Genomics[1] and Genetics of Deafness[2] Laboratories, The Wellcome Trust Sanger Institute, Hinxton, Cambridge CB10 1SA, United Kingdom

Received 17 July 2007/Returned for modification 29 August 2007/Accepted 15 December 2007

We have developed a bacterial artificial chromosome transgenesis approach that allowed the expression of myosin VIIa from the mouse X chromosome. We demonstrated the complementation of the *Myo7a* null mutant phenotype producing a fine mosaic of two types of sensory hair cells within inner ear epithelia of hemizygous transgenic females due to X inactivation. Direct comparisons between neighboring auditory hair cells that were different only with respect to myosin VIIa expression revealed that mutant stereocilia are significantly longer than those of their complemented counterparts. Myosin VIIa-deficient hair cells showed an abnormally persistent tip localization of whirlin, a protein directly linked to elongation of stereocilia, in stereocilia. Furthermore, myosin VIIa localized at the tips of all abnormally short stereocilia of mice deficient for either myosin XVa or whirlin. Our results strongly suggest that myosin VIIa regulates the establishment of a setpoint for stereocilium heights, and this novel role may influence their normal staircase-like arrangement within a bundle.

Sound perception and balance depend on the function of specialized sensory epithelial hair cells equipped with bundles of mechanosensory, microvillus-like cellular projections called stereocilia (42). Rows of stereocilia of increasing heights form a staircase-like arrangement organized into a V- or W-shaped bundle. Sound waves deflect bundles of stereocilia toward the taller row, which is believed to pull on tip links, opening transduction channels and leading to hair cell depolarization (22). The length, staircase-like organization, and bundle shape of stereocilia are critical for frequency selectivity and hair cell sensitivity. Each individual stereocilium is filled with hundreds of uniformly polarized and tightly cross-linked actin filaments. The actin filaments in each stereocilium core are oriented with the barbed ends (plus, polarizing ends) at its tip (10), and recent studies demonstrated that morphologically mature stereocilia undergo continuous turnover (40). The turnover of the actin core follows a treadmilling mechanism, and actin renewal rates are proportional to the lengths of stereocilia (39). However, the molecular bases for development of stereocilia, organization, and maintenance are not fully understood. Analyses of mouse models for deafness and balance defects indicate that formation of stereocilia, maintenance, and function depend on several proteins, including some of the known unconventional myosins.

Myosin VIIa is an unconventional myosin that, when lost or modified by mutation, is responsible for embryonic lethality and deafness in *Drosophila melanogaster* (26, 47), circling behavior in *Mariner* zebrafish mutants (11), hearing impairment and vestibular dysfunction in shaker1 mice, and hearing and retinal defects in human Usher syndrome 1B (13, 51). Myosin VIIa is expressed in sensory hair cells from the earliest stages of their development and localizes to their cytoplasm, apical parts, and stereocilia (15, 39). In mice homozygous for the *Myo7a*^{4626SB} allele, an *N*-ethyl-*N*-nitrosourea-induced recessive nonsense mutation which reduces the protein to below detectable levels (13, 16, 32), bundles of stereocilia show progressive morphological rearrangements from around embryonic day 18.5 (21, 41). Kros and colleagues (28) previously described raised thresholds for transduction currents and abnormal transduction channel gating in hair cells of myosin VIIa mutants, which could be explained by a reduced tension of tip links, thus resulting in a deafness phenotype. This reduced gating spring tension could reflect the properties of the tip link complexes and, more generally, the overall morphological rearrangements within mutant hair bundles. The molecular mechanism for the disorganization of stereocilia within shaker1 hair bundles remains unresolved and could be related to insufficient stereocilia coupling within a bundle, defects in their anchoring into the cuticular plate, or a perturbed regulation of actin dynamics affecting elongation of stereocilia during development (40). The elucidation of the role(s) of myosin VIIa in hair bundle development is therefore crucial to enhance our understanding of the underlying basis for the deafness phenotypes of shaker1 mice and Usher 1B syndrome in humans.

Using an X-chromosome-directed bacterial artificial chromosome (BAC) transgenic approach, we demonstrate genetic complementation of the *Myo7a*^{4626SB} allele (13, 16, 32). The embryonic stem (ES) cell-based BAC transgenesis method that we employed uses a recombination-mediated cassette exchange (RMCE) reaction whereby an "acceptor" locus of *loxP* and *lox5-11* sites is targeted within the hypoxanthine-guanine phosphoribosyltransferase (*Hprt*) gene on the X chromosome to act as docking sites for an extrachromosomal DNA molecule with similarly arrayed *lox* sites (19, 43). Many BAC vectors used for creating genomic libraries have such an arrangement of *lox* sites (12, 52). The *Hprt* locus was chosen because it has

* Corresponding author. Mailing address: The Wellcome Trust Sanger Institute, Wellcome Trust Genome Campus, Hinxton, Cambridge CB10 1SA, United Kingdom. Phone: 44 (0)1223 834244. Fax: 44 (0)1223 494919. E-mail: hmp@sanger.ac.uk.

† Supplemental material for this article may be found at http://mcb.asm.org/.

‡ H.M.P. and A.K.R. contributed equally to this article.

▽ Published ahead of print on 26 December 2007.

proven to be a reliable integration site for expression from tissue-specific promoters (4, 14), including expression from a human BAC clone (18). Some previously described methods for the Cre-mediated integration of genomic constructs at a single *loxP* site (5) entail integration of the entire genomic construct, including the vector backbone. The inclusion of prokaryotic sequences in transgene constructs has been implicated in the silencing of their expression in mice (6, 8). The RMCE reaction described here minimizes prokaryotic sequences at the transgene integration site.

The *Myo7a* BAC transgenes integrated at the *Hprt* locus are subject to X inactivation so that $Myo7a^{4626SB/4626SB}$ females carrying a hemizygous copy of the transgene exhibit mosaic expression of myosin VIIa within the inner ear sensory epithelium. The fine mosaic of myosin VIIa-deficient and -complemented hair cells allowed a direct comparison of phenotypic differences between the two hair cell populations within the same specimen, thereby eliminating variables such as genetic background, sampling strategy, and parallel processing/analysis. When directly compared with their complemented counterparts, stereocilia lacking myosin VIIa are significantly longer but shorten faster in the presence of an actin polymerization inhibitor. In addition, the loss of whirlin from tips of stereocilia that normally occurs during hair bundle maturation was delayed, and this correlated with elevated levels of its immunofluorescence in myosin VIIa-deficient cells. Our results strongly suggest that myosin VIIa plays a regulatory role in setting the appropriate heights of stereocilia and demonstrate that X-linked BAC transgenic mouse lines provide a useful tool for studying gene function, as they can significantly enhance the resolution of phenotypic analyses.

MATERIALS AND METHODS

Vector construction and BAC manipulation. An *Hprt* targeting construct was generated in a pBluescript SKII(+) (Stratagene)-based backbone vector containing a modified polylinker and an *MC1-DTA*-negative selection marker. Genomic sequences from the *Hprt* gene of 129S7/SvEv origin were cloned as homologous arms on either side of a puromycin resistance-thymidine kinase fusion gene (*puΔtk*) cassette (7) flanked by directionally opposed *loxP* and *lox5-11* sites to create construct pCCI18; the 5′ arm was a 2.5-kb EcoRV/HindIII fragment from vector pRIV6.9PGK, and the 3′ arm was a 2.7-kb HindIII/BamHI fragment from vector pIV7.1 (17).

Four BAC clones were used in this study: zebrafish (RPCI 71-30I22) and human (RPCI 11-189K21) BACs were used in the initial phase of establishing and validating BAC integration into ES cells, whereas BACs containing *Myo7a* (RPCI 23-138G2 and RPCI 24-233J11) were used for complementation in mice. The cloning vectors used in the four BAC clones, either pBACe3.6 or pTARBAC1, both contained *loxP* and *lox5-11* sites flanking the genomic insert and the *sacBII* gene (12, 52). The vector backbones were modified by insertion of the *pgk/EM7 Neo/Kan*^{R}-positive selection cassette (pCEI1) into the *sacBII* gene by bacterial homologous recombination. pCEI1 was generated by PCR of homologous arms of *sacBII* sequences with Hi-Fidelity Supermix (Invitrogen) as follows: the 5′ arm (bp 3110 to 3609) of pBACe3.6 was amplified with primers *sacBII*1A (AACGAAAAATACCAAGTGCCTCAA) and *sacBII*1B (GATATG TTTTTCCGTCTCCGTCAA), and the 3′ arm (bp 3736 to 4179) of pBACe3.6 was amplified with primers *sacBII*3A (AAAACGGATACCAAGGCGAAGA ATC) and *sacBII* 3B (CTGCGAAGTGAGAGTAAGTGAATG), followed by restriction enzyme digestion (HindIII/EcoRI for the 5′ arm and SpeI/BamHI for the 3′ arm) and four-way ligation into vector PL450 (31). The recombineering cassette was amplified by PCR using primers *sacBII*1A and *sacBII*3B and gel purified (Qiagen gel purification kit). BAC clones were modified in *Escherichia coli* EL350 cells (31). BAC clones were retransformed into *E. coli* DH10B cells for large-scale DNA preparation.

Recombination was confirmed by Southern analysis of BAC DNA using *Kan*^{R} gene- or homology arm-specific DNA probes. Additionally, for modification of *sacBII*, pulsed-field gel analysis was performed on 1 μg of NotI-digested BAC DNA using a Bio-Rad CHEF mapper (an initial switch time of 4 s, a final switch time of 17.3 s, a gradient of 6 V cm^{-1}, and a run time of 18.3 h). A Qiagen large-construct kit was used for the preparation of modified BAC DNA. DNA was resuspended in Tris-EDTA buffer and concentrated by evaporation to approximately 1 μg ml^{-1}.

ES cell culture. ES cell cultures, electroporation, mini-Southern-blot analysis of ES cell clones, and the generation of chimeric and germ line mice were described previously (37). The male 129S7/SvEvBrd-*Hprt*$^+$ ES cell clone AB1 was used for targeting. ES cells (0.9×10^7 cells) were electroporated (500 μF, 230 V; Bio-Rad) with PmeI-linearized pCCI18 (10 μg) and selected after 24 h using puromycin (3 μg ml^{-1}). Southern analysis was performed using a 5′ external probe, a 400-bp BamHI/XmnI fragment isolated from clone RIV6.9IPGK, and a 3′ external probe, a 0.7-kb HindIII/PstI fragment from clone phpt2 (17). The drug selection sensitivities of homologous recombinant $hprt^{tm(rmce1)Brd}$ ES clones to hypoxanthine-aminopterin-thymidine, 6-thioguanine (6-TG), puromycin, and G418 were assessed.

For RMCE integration of BAC inserts into $hprt^{tm(rmce1)Brd}$, 3×10^7 cells were electroporated (500 μF, 230 V; Bio-Rad) with various amounts of BAC DNA and 25 μg pCAGGS-*Cre* (1). The selection of ES cell clones with G418 (200 μg ml^{-1}) began 24 h after transfection and proceeded for 5 to 6 days. Subsequently, selection with 6-TG (10 μM) proceeded for 3 to 4 days, at which time double-resistant colonies were isolated. BAC integration was verified by Southern analysis using the 5′ external probe and a 3′ internal probe (400-bp EcoRI/XhoI fragment from clone IV7.1PGK) (17).

BAC integrity was analyzed by PCR under standard conditions (Platinum *Taq*; Invitrogen). Annealing temperatures were as follows: 50.0°C for RPCI 71-30I22 primer pairs 2, 5, and 7 and the mouse-specific control, 54.0°C for primer pairs 1, 3, 6, and 8, 58.0°C for primer pair 4, and 52.5°C for all RPCI 11-189K21 primer pairs. BAC integration was visualized by fluorescence in situ hybridization (FISH) analysis on metaphase spreads of ES cells (24). BAC probes were fluorescein isothiocyanate-labeled zebrafish (RPCI 71-30I22) and Texas Red-labeled mouse (RPCI 23-156G14) *Hprt*.

Mouse breeding and behavioral analyses. All animal studies were licensed by the United Kingdom Home Office under the Animals (Scientific Procedures) Act of 1986 and approved by the local ethics committee. To test for complementation, $Myo7a^{4626SB/4626SB}$ males were bred with $Myo7a^{4626SB/+}$ $Hprt^{(Myo7a)Brd/+}$ females. Offspring were of mixed CBA/Ca, 129S7, C3H, and C57BL/6J genetic backgrounds. Mice were genotyped by PCR for the $Myo7a^{4626SB}$ allele (21) and by Southern blotting with the *Hprt* 3′ internal probe (see Appendix S1 in the supplemental material for an alternative PCR-based genotyping method for the BAC transgene). PCR-based genotyping does not determine the homozygosity of the $Myo7a^{4626SB}$ allele, as wild-type *Myo7a* is also present in BAC transgenic animals. Therefore, candidate complemented mice were selected based on the presence of BAC and the absence of a shaker1 vestibular phenotype. To confirm complementation, candidate BAC transgenic mice were test bred with wild-type C57BL/6J mice in order to establish whether they were $Myo7a^{4626SB/4626SB}$ based on the genotypes of offspring. Hearing was assessed using a Preyer's reflex (flick of the pinna) in response to a 19.5-kHz tone burst at an intensity of 90 dB sound pressure level, and vestibular function was evaluated based on behavior (circling, head bobbing, and hyperactive locomotion indicating vestibular dysfunction).

SEM. For scanning electron microscopy (SEM) analyses, cochleae from adult mice at postnatal day 28 (P28) were fixed for 3 h with 2.5% glutaraldehyde in 1 mM sodium cacodylate buffer (pH 7.4). Samples were then washed in phosphate-buffered saline, processed with the OTOTO (osmium-thiocarbohydrazide-osmium-thiocarbohydrazide-osmium) method, adapted from a method described previously by Hunter-Duvar (23), dehydrated in ethanol, critical-point dried (BalTec), and viewed with an S-4800 scanning electron microscope (Hitachi) at 3 to 5 kV. A summary of mice used for experimentation is provided in Appendix S2 in the supplemental material.

Histochemistry. Myosin VIIa was immunolocalized in cochleae isolated from mice at P5 and fixed in 4% paraformaldehyde using polyclonal anti-myosin VIIa antibody (Proteus BioSciences). Myosin XVa and whirlin were localized using antibodies PB48 and HL5141, respectively (3, 30), at P7, P15, and P28. Stereocilium dimensions and pixel intensity values (in arbitrary intensity units) were measured with NIH ImageJ software. Hair cells (10 to 30 cells for each genotype) from the middle turn of the cochlea were analyzed, and only the most lateral (tallest-row) stereocilia were evaluated (at least one cochlea of at least four animals of each genotype). Analyses of the dimensions of stereocilia were focused on the most lateral row, as it was not possible to unambiguously determine to which row the shorter stereocilia of the disorganized shaker1 hair bundles belonged. SEM images were obtained at the same distance from the detector and

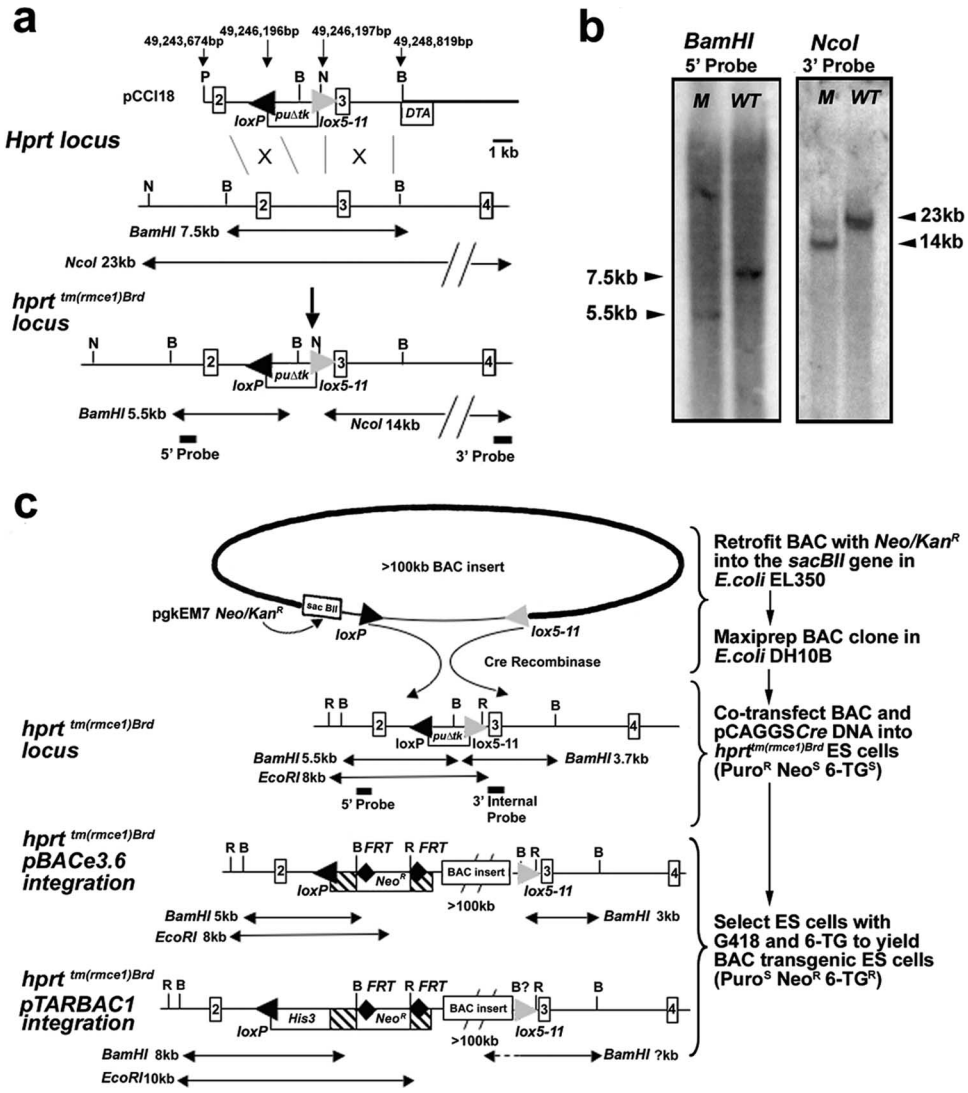

FIG. 1. Modifying the *Hprt* locus to allow BAC insert integration by RMCE. (a) Targeting construct pCCI18 linearized with PmeI was homologously recombined into intron 2 of the *Hprt* locus to generate ES cell clones with the RMCE acceptor allele $hprt^{tm(rmce1)Brd}$. X-chromosome base pair coordinates for the targeting vector and RMCE cassette are indicated (NCBI m36 and Ensembl v42). Correct targeting was determined using NcoI digestion with the use of the 3′ probe and BamHI digestion with the use of a 5′ probe. P, PmeI; N, NcoI; B, BamHI; *puΔtk*, puromycin resistance-truncated thymidine kinase fusion gene. (b) Southern analysis of *Hprt* targeting using 5′ and 3′ flanking probes. M, $hprt^{tm(rmce1)Brd}$ ES cell clone; WT, wild-type ES clone. (c) Integration of BAC inserts into the $hprt^{tm(rmce1)Brd}$ locus is schematically depicted. The BACs were modified with the *pgkEM7 Neo/Kan*^{R} cassette from plasmid pCEI1 in *E. coli* EL350. DNA for the BACs was prepared from *E. coli* DH10B cells and electroporated into ES cells carrying the $hprt^{tm(rmce1)Brd}$ allele. The alternative Southern blot genotyping strategies for pBACe3.6 and pTARBAC1 vector-based BAC clones are depicted. R, EcoRI; B, BamHI; Neo/Kan^R, neomycin and kanamycin resistance gene. The sensitivities (superscript S) and resistances (superscript R) of ES cell clones to the drugs puromycin (Puro), Neomycin (Neo), and 6-TG are indicated in the flow diagram on the right. BamHI ?kb indicates that for pTARBAC1 vectors, the size of the diagnostic BamHI fragment is not consistent between individual BAC clones and must be determined empirically or by prediction, if the BAC clone sequence is known. The 3′ internal probe was used for subsequent genotyping of ES cell-derived mouse lines.

from samples mounted at comparable angles. Two-tailed *t* tests were performed using Excel software.

Organotypic cultures of mouse organ of Corti at P4 were prepared as previously described (39). For the cytochalasin D experiments, organ of Corti cultures from one ear were incubated for 16 h with Dulbecco's modified Eagle's F-12 medium containing 0.025 μM cytochalasin D from a 0.05 mM ethanol stock (Sigma), while the other ear of the same animal was incubated with an equivalent amount of ethanol (1.5 μl per 3 ml of medium). Cultures were then processed as previously described (39), and actin filaments were stained with Alexa Fluor 488/phalloidin and analyzed using a Zeiss LSM 510 confocal microscope (Zeiss) with a 63× 1.4-numerical-aperture objective.

A summary of mice used for experimentation is provided in Appendix S2 in the supplemental material.

***Myo7a-lacZ* mice.** A full description of the generation and analysis of *Myo7a-lacZ* transcriptional reporter mice is contained in Appendix S7 in the supplemental material.

RESULTS

BAC integration at the *Hprt* locus by RMCE. An acceptor locus was generated by targeting an RMCE cassette into the single *Hprt* locus in AB1 male ES cells, creating the $hprt^{tm(rmce1)Brd}$ allele (Fig. 1a and b). The targeted ES cells retained hypoxanthine-aminopterin-thymidine resistance and 6-TG sensitivity

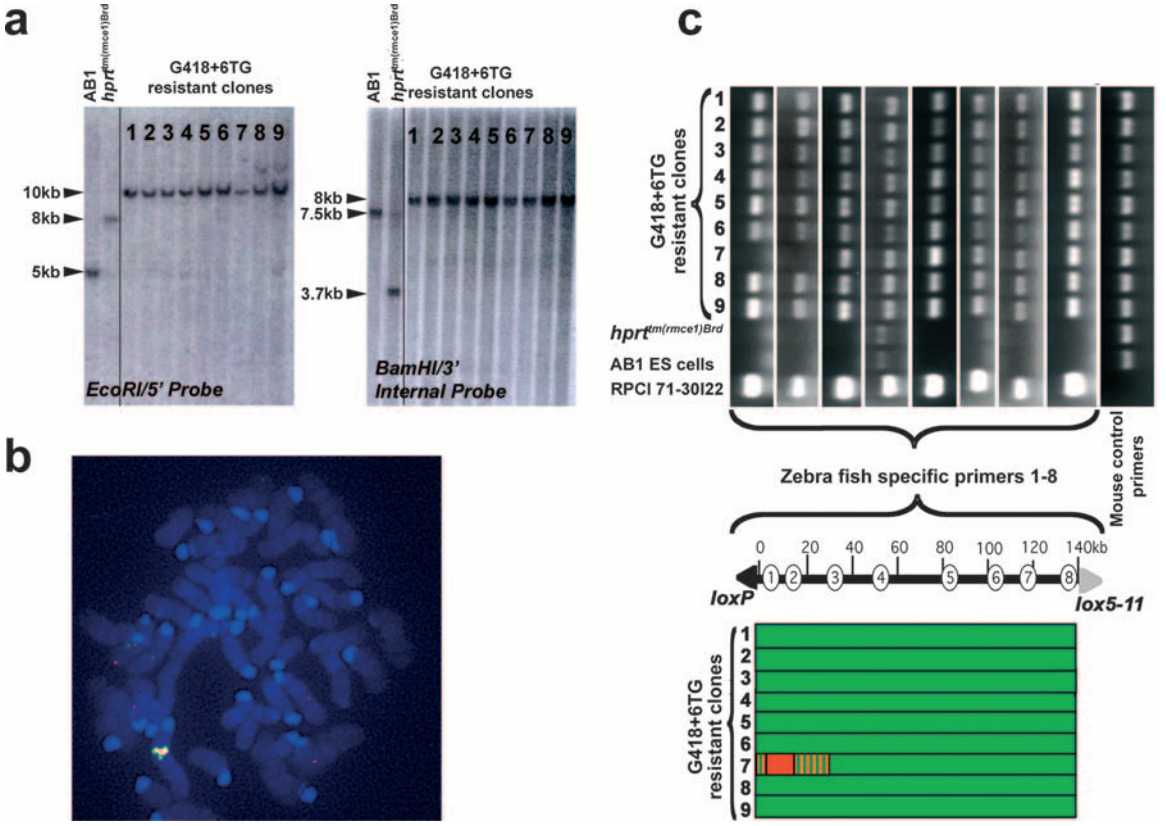

FIG. 2. Testing efficiency and integrity of BAC integration at the *hprt*$^{tm(rmce1)Brd}$ acceptor locus using a zebrafish BAC clone. (a) Southern analysis with 3′ internal and 5′ flanking probes. (b) FISH analysis of an ES cell metaphase spread showing colocalization of the zebrafish BAC RPCI 71-30I22 (fluorescein isothiocyanate) (green) and the mouse *Hprt* locus containing BAC RPCI 23-156G14 (Texas Red). (c) PCR analysis for BAC integrity using eight primer pairs internal to the RPCI 71-30I22 sequence (GenBank accession number AL590148) and control primers that amplified the mouse genomic sequence. The PCR analysis is schematically depicted as solid green bars for an intact BAC sequence within an individual ES cell clone; red bars depict a gap, and striped bars indicated that the extent of the gap is unknown.

and acquired puromycin resistance. Bacterial recombination based on the λred system (29, 31) was used to insert the kanamycin resistance gene into the *sacBII* gene present in the backbone of multiple vectors (Fig. 1c; see Appendix S3 in the supplemental material). A combination of G418 positive selection for integration of the BAC sequence followed by 6-TG negative selection for *Hprt* gene-specific integration can thus be employed to specifically select for the RMCE event (Fig. 1c).

Our initial experiments were directed at establishing and validating BAC integration using clones of known sequence from species other than mouse. The zebrafish BAC clone (RPCI 71-30I22), with a 141-kb insert size, was cotransfected with pCAGGS-*Cre* (1) into an *hprt*$^{tm(rmce1)Brd}$ cell line by electroporation (40 μg of BAC and 20 μg of pCAGGS-*Cre*, giving a molar ratio of 1:12). This yielded nine double (G418 and 6-TG)-resistant ES cell clones, estimated as approximately 2% of the total G418-resistant ES clones (as plating 20% of the transfected cells yielded gave 117 colonies with G418 selection alone). Using Southern analysis with *Hprt* flanking probes and metaphase FISH analysis with differentially labeled RPCI 71-30I22 and a mouse *Hprt* locus BAC, we demonstrated *Hprt* integration of RPCI 71-30I22 by RMCE in all G418 and 6-TG double-resistant ES clones, with no evidence of BAC integration at other loci (Fig. 2a and c; data not shown). A similar analysis was performed using a 151-kb human BAC clone (RPCI 11-189K21), except that 25 μg of pCAGGS-*Cre* was used each time in multiple transfections, with the BAC quantity titrated as indicated in Appendix S4 in the supplemental material. Southern analysis of the 36 surviving G418 and 6-TG double-resistant ES cell clones showed that 30 of them had completed RMCE events at the *hprt*$^{tm(rmce1)Brd}$ allele (see Appendix S5 in the supplemental material). Of the remainder, two ES cell clones showed a deletion within the *hprt*$^{tm(rmce1)Brd}$ allele without site-specific BAC integration. Additionally, four BAC transgenic ES cell clones showed 3′ *Hprt* flanking fragments that indicated that the RMCE reaction did not proceed to completion in some or all of the ES cells within each clone. This created an insertion, or a "pop-in," of the entire BAC clone at the single *loxP* site of the *hprt*$^{tm(rmce1)Brd}$ allele. The pop-in events occurred in clones originating from transfections performed using all four of the molar ratios of BAC to pCAGGS-*Cre* that were used.

We used the same zebrafish and human BAC transgenic ES cell clones to analyze the integrity of the heterologous DNA sequences integrated within the mouse *Hprt* locus. The integrated zebrafish BAC clone (RPCI 71-30I22) was analyzed using eight PCR primer pairs with genomic targets spaced at

10- to 20-kb intervals (Fig. 2b; see Appendix S6 in the supplemental material). Of the nine ES cell clones analyzed, eight contained intact BAC inserts and one had a deletion. For the 34 ES cell clones with the integrated human BAC (RPCI 11-189K21), a total of 33 PCR primer pairs were used (see Appendices S5 and S6 in the supplemental material). Twenty-two clones (65% of the total) appeared to be intact at the resolution of this analysis, while 12 clones carried a variety of deletions.

BAC transgenesis and complementation of the shaker1 mutation. BAC clones from the C57BL/6J mouse strain containing the *Myo7a* gene (RPCI 23-138G2 and RPCI 24-233J11) were chosen for transgenesis (Fig. 3a). As a reporter for *Myo7a* transcription, RPCI 23-138G2 was modified by the integration of an *E. coli lacZ* gene. Analysis of the $hprt^{(Myo7a\text{-}lacZ)Brd}$ transgenic mouse line demonstrated that expression from the X chromosome within the inner ear was specifically in hair cells and persisted beyond 6 months of age (see Appendix S7 in the supplemental material). In order to complement the shaker1 phenotype of the $Myo7a^{4626SB}$ allele, a total of five transgenic mouse lines were created for two different *Myo7a*-containing BAC clones (see Appendix S8 in the supplemental material). From these five transgenic lines, two independent BAC transgenic lines for RPCI 23-138G2 (*Myo7a* BAC C11 and *Myo7a* BAC C9) and a single line for RPCI 24-233J11 (*Myo7a* BAC D7) were bred into the *Myo7a* mutant background. The breeding strategy culminated in a cross between a $Myo7a^{4626SB/4626SB}$ male and a $Myo7a^{4626SB/+}$ female carrying the BAC transgene on an X chromosome so that half of the resulting offspring were expected to give a shaker1 phenotype in the absence of complementation. The offspring carrying at least one $Myo7a^{4626SB}$ allele and a BAC transgene, but showing no circling and head bobbing (indicative of vestibular dysfunction), were found in two out of three of the *Myo7a* BAC transgenic lines, namely, *Myo7a* BAC C11 and line *Myo7a* BAC D7, and complementation was confirmed by test breeding (see Appendix S9 in the supplemental material). Mice from both of these BAC transgenic lines were analyzed further, with the allele being collectively referred to as $hprt^{(Myo7a)Brd}$. The third BAC transgenic line, *Myo7a* BAC C9, did not yield any complemented mice, presumably due to a deletion within the BAC that affected the normal function of the *Myo7a* gene.

The bundles of stereocilia on the apical surfaces of auditory hair cells of $Myo7a^{4626SB/4626SB}$ mice that were either $Hprt^{(Myo7a)Brd/Y}$ males or $Hprt^{(Myo7a)Brd/(Myo7a)Brd}$ females were indistinguishable from those of $Myo7a^{4626SB/+}$ and wild-type mice in terms of bundle shape, orientation, and the presence of tip links and horizontal top connectors between adjacent stereocilia, confirming the successful complementation of the $Myo7a^{4626SB/4626SB}$ phenotype (Fig. 3b and c and 4a and data not shown). Moreover, we did not find any alterations of the cellular arrangement of inner ear epithelia or the morphology of hair bundles in any of the cochleae of $Myo7a^{+/+}$ or $Myo7a^{4626SB/+}$ mice carrying either one or two copies of the *Myo7a* BAC transgene (data not shown), which suggests either that an excess of myosin VIIa has no adverse effect or that protein levels are closely regulated. $Myo7a^{4626SB/4626SB}$ $Hprt^{(Myo7a)Brd/+}$ mice showed a very fine intermixing of complemented and mutant hair cells due to the process of female X-chromosome inactivation.

Myosin VIIa plays a regulatory role in the dynamics of actin of stereocilia. The fine mosaic of myosin VIIa-deficient and complemented hair cells in the inner ear epithelia of female mice hemizygous for the BAC transgene allowed direct side-by-side comparisons of affected and complemented hair cells. Detailed SEM analyses performed on inner hair cells from the middle turn of the mosaic cochlea (approximately 50% of cochlear length) demonstrated that the width (0.40 ± 0.05 μm; $n = 293$; $P = 9.9 \times 10^{-22}$ by *t* test) and length (3.02 ± 0.57 μm; $n = 323$; $P = 1.8 \times 10^{-5}$ by *t* test) of the most lateral (tallest) stereocilia on mutant inner hair cells were significantly increased relative to those of myosin VIIa-complemented inner hair cells in the immediate vicinity (0.36 ± 0.03 μm [$n = 338$] and 2.07 ± 0.43 μm [$n = 378$]) (Fig. 4a and b). The analysis of mosaic auditory epithelia enabled us to visualize differences in dimensions of stereocilia that were not large enough to be detected in previous studies of shaker1 mice (41). The length of the stereocilia of inner hair cells complemented by transgenically expressed myosin VIIa did not differ significantly from those of wild-type animals when hair cells from the corresponding regions of the cochlea were compared (2.09 ± 0.25 μm; $n = 263$; $P = 0.5$ by *t* test). Consistent with previous studies (41), the number of stereocilia in the most lateral (tallest) row was significantly reduced in mutant inner hair cells (22 lateral row stereocilia per bundle [±4.5]; $n = 63$; $P = 1.4 \times 10^{-38}$ by *t* test) relative to adjacent *Myo7a*-complemented inner hair cells (34 lateral row stereocilia per bundle [±1.7]; $n = 59$).

The actin core of the mature stereocilium undergoes continuous turnover while its length is maintained in a dynamic steady state (39, 40). However, to promote elongation of stereocilia during development, the polymerization rates of actin filaments must exceed their depolymerization rates until the stereocilia reach their predetermined lengths. In the shaker1 mutants, the myosin VIIa deficiency within the cuticular plate (a dense, actin-rich structure at the apex of each hair cell) and at the bases of stereocilia could result in decreased rates of actin depolymerization and greater elongation of stereocilia. To investigate the rates of actin depolymerization in developing shaker1 hair bundles, we blocked actin polymerization with cytochalasin D (39) in cultured auditory epithelia harvested from P4 $Myo7a^{4626SB/4626SB}$ $Hprt^{(Myo7a)Brd/+}$ females mosaic for myosin VIIa expression. In untreated explants from the corresponding regions of the other ear of each mouse, the myosin VIIa-deficient stereocilia of the lateral rows were significantly longer than the stereocilia of adjacent hair cells expressing myosin VIIa, consistent with our SEM observations of adult mice. However, upon 16 h of cytochalasin D treatment, the differences in lengths of stereocilia between myosin VIIa-deficient and -complemented hair cells were dramatically reduced (Fig. 4c and d), indicating that actin depolymerization rates were higher in the absence of myosin VIIa rather than lower.

The excessive elongation of myosin VIIa-deficient stereocilia could be explained by elevated rates of actin polymerization in the stereocilium core. Therefore, we analyzed the localization of two proteins implicated in elongation of stereocilia, myosin XVa and whirlin (3, 20, 27, 33), in myosin VIIa-deficient hair cells. Both myosin XVa and whirlin were found in the tips of both myosin VIIa-deficient and -complemented stereocilia at P7. The intensity

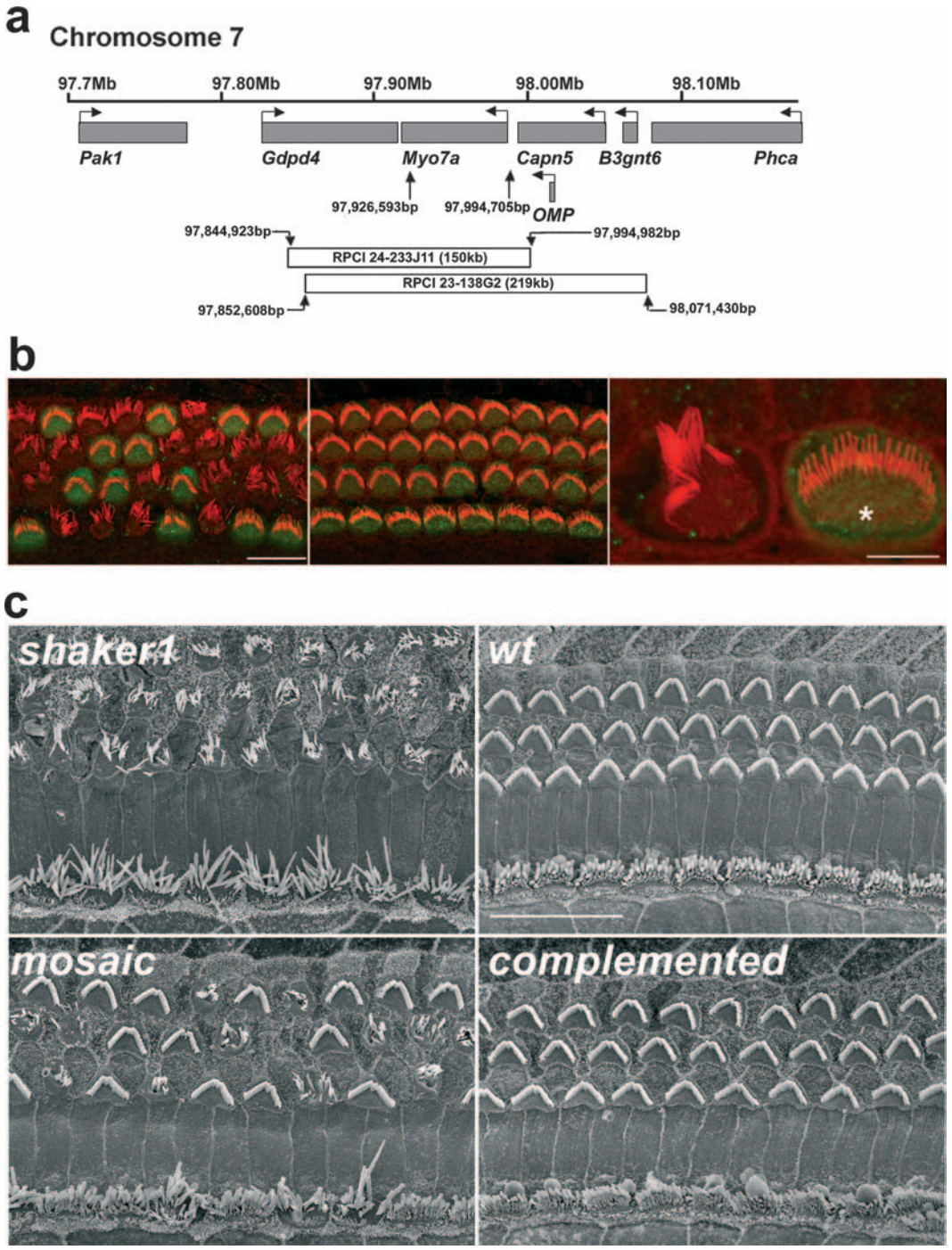

FIG. 3. Myosin VIIa expressed from the X chromosome complements the sensory epithelium of shaker1 mice. (a) Schematic of the relative position of the *Myo7a* genomic locus relative to those of other genes in the vicinity and the BAC clones used for transgenesis: RPCI 23-138G2 and RPCI 24-233J11 (GenBank accession number AC115022). Chromosome 7 base pair coordinates for *Myo7a* and the BAC clones are shown (NCBI m36 and Ensembl v42). The *Myo7a* transcriptional start is defined under GenBank accession number AF384559. (b) Myosin VIIa immunoreactivity (green) coincided with the complementation of hair bundles in mosaic (left) and fully complemented (middle) auditory epithelia at P5. The high-resolution confocal image (on the right) shows a well-organized hair bundle and myosin VIIa immunoreactivity at the apex of a complemented cell (*), while an adjacent myosin VIIa-negative cell exhibits disorganized stereocilia. Actin filaments in stereocilia were counterstained with rhodamine/phalloidin (red). Scale bars, 10 μm (left and middle) and 2.5 μm (right). (c) Comparison of SEM images of auditory sensory epithelia of $Myo7a^{4626SB/4626SB}$ (shaker1), $Myo7a^{+/+}$ (wild type), female $Myo7a^{4626SB/4626SB}$ $Hprt^{(Myo7a)Brd/+}$ (mosaic), and female $Myo7a^{4626SB/4626SB}$ $Hprt^{(Myo7a)Brd/(Myo7a)Brd}$ (complemented) mice at P28. The $Myo7a^{4626SB/4626SB}$ hair bundles of outer and inner hair cells were severely disorganized compared to those of wild-type mice. The apical surfaces of the auditory epithelia of complemented mice were indistinguishable from those of wild-type mice, while mosaic females showed a fine mixing of disorganized and complemented hair bundles. Scale bars, 30 μm.

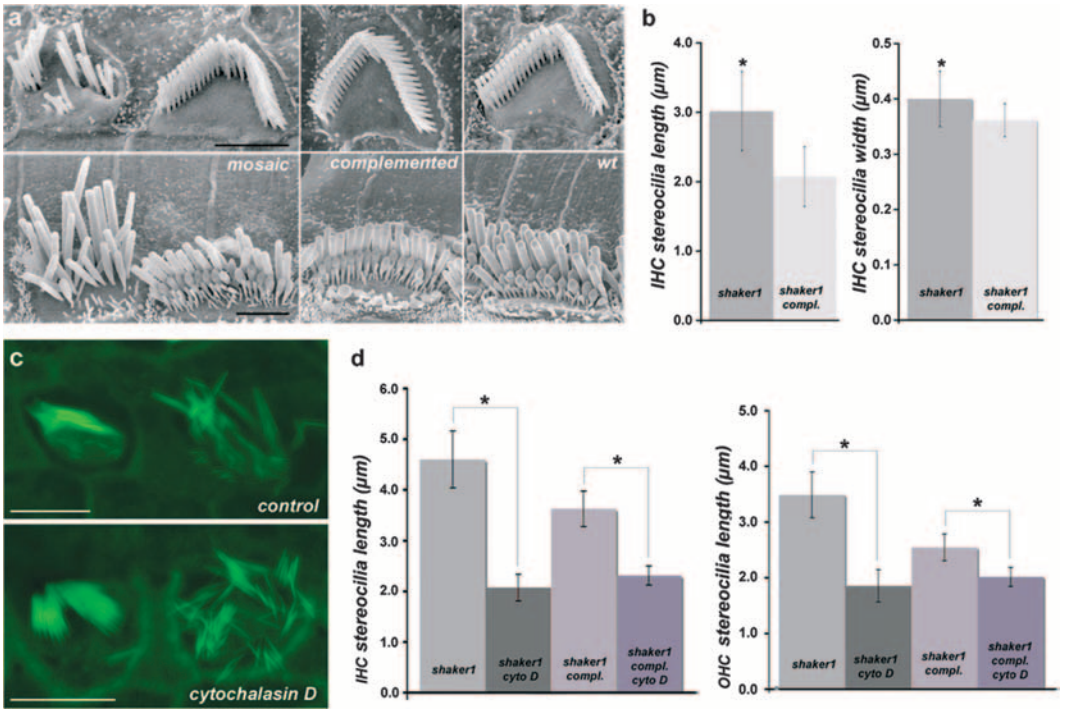

FIG. 4. Complemented hair cells are indistinguishable from those of wild-type mice and allow fine analysis of the shaker1 phenotype in mosaic females. (a and b) The successful complementation (compl.) of the shaker1 phenotype in a subpopulation of hair cells within mosaic *Myo7a*$^{4626SB/4626SB}$ *Hprt*$^{(Myo7a)Brd/+}$ auditory epithelia (left, outer hair cells [top image] and inner hair cells [bottom image]) allowed a detailed SEM comparison between adjacent cells (a), revealing an increase in length of myosin VIIa-deficient inner hair cell (IHC) stereocilia at P28 (b). For consistency, only the single row of the most lateral (tallest) stereocilia in each bundle was measured. For comparison, images of a representative outer hair cell from a complemented male [*Myo7a*$^{4626SB/4626SB}$ *Hprt*$^{(Myo7a)Brd/Y}$] and an inner hair cell from a fully complemented female [*Myo7a*$^{4626SB/4626SB}$ *Hprt*$^{(Myo7a)Brd/(Myo7a)Brd}$] (a, middle, top, and bottom images, respectively) and outer and inner hair cells from wild-type (*Myo7a*$^{+/+}$) mice (a, right, outer hair cells [top image] and inner hair cells [bottom image]) are provided. Confocal analyses revealed that in cultured epithelia at P4, the longer myosin VIIa-deficient stereocilia (c, right) shortened faster in the presence of cytochalasin D than did stereocilia of complemented (c, left) inner hair cells (c, bottom, and d) compared to controls treated with an ethanol carrier (c, top, and d). Measurements for shaker1 (sh1) inner hair cells (IHC) were 4.60 ± 0.56 μm for the ethanol control (eth. contr.) and 2.07 ± 0.26 μm for cytochalasin D (cyto. D) ($P = 5.5 \times 10^{-59}$ by *t* test); measurements for shaker1 outer hair cells (OHC) were 3.49 ± 0.41 μm for the ethanol control and 1.86 ± 0.29 μm for cytochalasin D ($P = 9.6 \times 10^{-36}$ by *t* test); measurements for complemented inner hair cells were 3.63 ± 0.35 μm for the ethanol control and 2.31 ± 0.19 μm for cytochalasin D ($P = 4.8 \times 10^{-18}$ by *t* test); measurements for complemented outer hair cells were 2.54 ± 0.24 μm for the ethanol control and 2.02 ± 0.17 μm for cytochalasin D ($P = 2.9 \times 10^{-14}$ by *t* test). An asterisk represents a significant difference ($P < 0.01$). Actin filaments shown in panel c were stained with Alexa Fluor 488/phalloidin. Scale bars, 2 μm (a) and 5 μm (c).

of myosin XVa immunofluorescence was graded with stereocilium lengths, as previously described for control animals (39), while the intensities of whirlin labeling were comparable across the bundle of stereocilia (Fig. 5a) (3, 27). However, at P7, the whirlin-specific immunofluorescence measured at the level of the cuticular plate was elevated in hair cells lacking myosin VIIa compared to their complemented counterparts within mosaic epithelia (Fig. 5a). In *Myo7a*$^{4626SB/+}$ mice, whirlin immunolabeling at the tips disappears from shorter stereocilia during morphological maturation of the bundle (3, 27). In myosin VIIa-complemented hair cells at P15 and P28, whirlin immunofluorescence recapitulated the distribution obtained previously with this antibody in wild-type adult mice and was observed only in the tips of the most lateral stereocilia of inner hair cells but was absent from the shorter stereocilia of the second and subsequent rows within the same bundle and from all outer hair cell stereocilia (Fig. 5a, top right). Surprisingly, however, whirlin immunoreactivity persisted across the mature bundles of stereocilia of both inner and outer hair cells lacking myosin VIIa at P15 and P28, irrespective of the length of individual stereocilia (Fig. 5a and data not shown). To further evaluate possible interactions between myosin VIIa and whirlin, we analyzed the spatial distribution of myosin VIIa within the auditory sensory epithelia of shaker2 and whirler mutants lacking myosin XVa and whirlin, respectively (2, 20, 33, 36). Although overall myosin VIIa-specific immunofluorescence showed comparable levels in the cytoplasms of mutant and control hair cells (data not shown), we detected myosin VIIa at the tips of the abnormally short stereocilia of both *Whrn*$^{wi/wi}$ and *Myo15*$^{sh2/sh2}$ mice. In the lateral row of stereocilia of *Whrn*$^{wi/+}$ and *Myo15*$^{sh2/+}$ mice, the myosin VIIa labeling was restricted to the sides of stereocilia (Fig. 5b) and was absent from the tips, as previously described (15, 39). However, we were able to detect myosin VIIa in the tips of the shorter stereocilia within the same bundles of *Whrn*$^{wi/+}$ and *Myo15*$^{sh2/+}$ (Fig. 5b, inset) and wild-type (data not shown) mice.

DISCUSSION

Site-specific BAC insert integration at the *Hprt* locus is selected efficiently. The approach for the integration of BAC

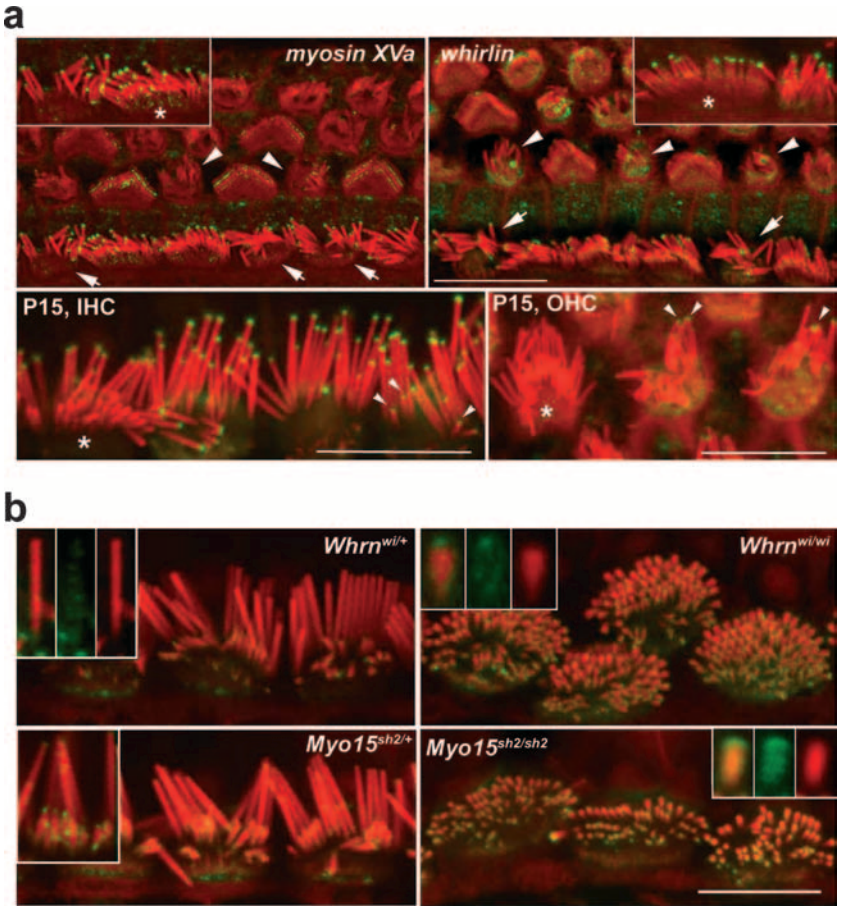

FIG. 5. Both myosin XVa and whirlin localize to the tips of myosin VIIa-deficient stereocilia, but the whirlin labeling pattern persists abnormally during bundle development. (a) Myosin XVa and whirlin localized (green) to the tips of stereocilia of myosin VIIa-deficient inner (arrows), outer (arrowheads), and complemented hair cells at P7. Insets show representative inner hair cells at a higher magnification; complemented hair cells are indicated by asterisks. Interestingly, whirlin could still be observed in the tips of all myosin VIIa-deficient stereocilia at P15 (bottom, inner hair cells [IHC] and outer hair cells [OHC]) while being restricted to the most lateral stereocilia of complemented inner hair cells (*). Note the elevated levels of whirlin immunoreactivity in the cuticular plates of cells lacking myosin VIIa (pixel intensity values in arbitrary units for mutant outer hair cells are 27.24 ± 2.88, [$n = 34$] for complemented outer hair cells and 16.70 ± 2.09 [$n = 27$] for mutant outer hair cells [$P = 2.5 \times 10^{-22}$ by t test]). (b) In mice heterozygous for whirler ($Whrn^{wi/+}$) and shaker2 ($Myo15^{sh2/+}$) alleles, myosin VIIa (green) is present along the length of the most lateral (tallest) stereocilia (top, left inset) and at the tips of the shorter stereocilia (bottom, left inset). In the abnormally short stereocilia of mice lacking whirlin ($Whrn^{wi/wi}$) and myosin XVa ($Myo15^{sh2/sh2}$), myosin VIIa localizes at the tips. Insets show isolated stereocilia at a high magnification; merged images on the left show a green channel in the middle and a red channel on the right. Actin filaments in stereocilia were counterstained with rhodamine/phalloidin (red). Scale bars, 10 μm.

inserts that we have adopted is based on RMCE using two inverted *lox* sites that are already present in many vector backbones used for genomic libraries (12). The individual BAC clones only require modification using a standardized and efficient recombineering reaction in order to insert a positive selection cassette (29, 31). The positive/negative dual selection ensures that the Cre-mediated integration of the BAC into the *Hprt* locus occurs with a very low background of randomly integrated BACs. Analyses using BACs containing heterologous sequences indicate that the majority of integrated BAC inserts are intact. It is likely that the deletions that we observed were introduced as a result of DNA strand breakage during BAC isolation or transfection, as there was little evidence of de novo deletion during BAC propagation or recombineering.

We envisage that the technique of RMCE integration of BACs could be particularly useful where control over copy number and integration site is desirable. One example might be the creation and phenotypic analysis of an allelic series of engineered transgene variants within mice or ES cells (38, 48). The minimal manipulation required also makes this approach an attractive alternative to targeted knock-in for creating transcriptional reporters or fusion proteins with a variety of tags and "humanizing" mice by gene addition on a null mutant background or by syntenic replacement (50).

X-inactivation mosaicism as a tool in cell biology research. Chimeras and mosaics provide a means to create mice containing two genetically distinct cell populations that can enhance the information on gene function that can be obtained from null mutant studies alone; for example, we can ask about the contribution of mutant cells to particular tissues during development or whether a gene functions cell autonomously (35, 46). Currently available strategies each have their own

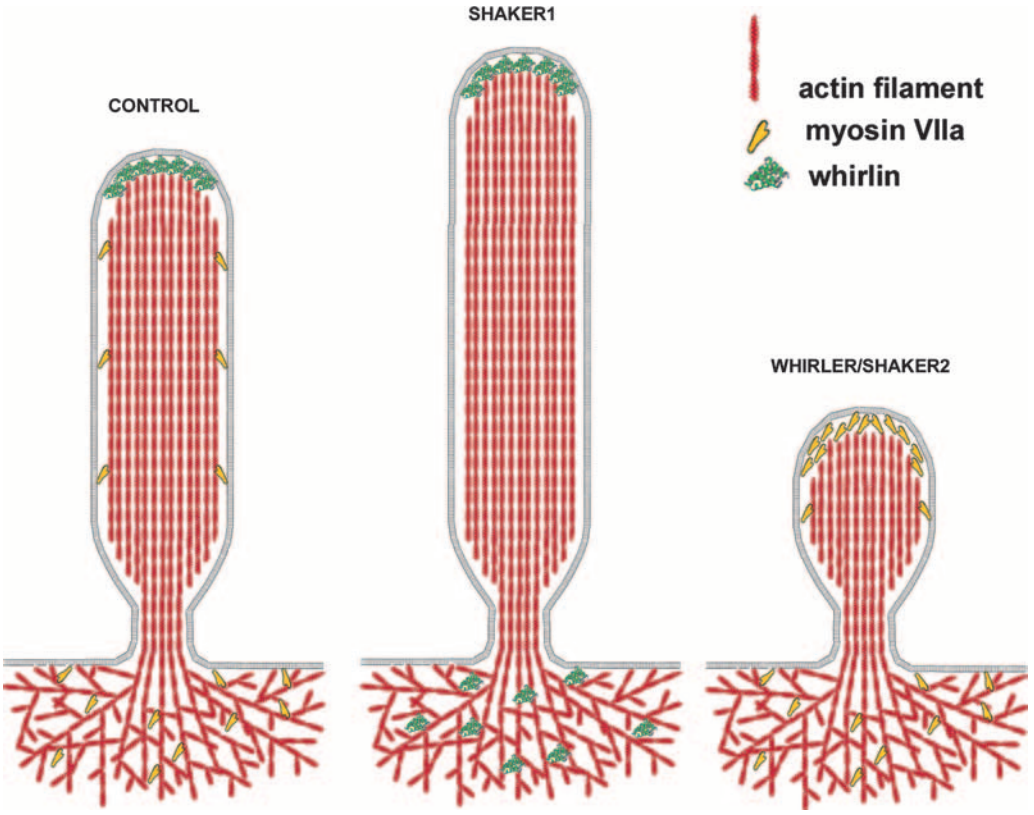

FIG. 6. Diagram of myosin VIIa and whirlin distribution in control shaker1 and whirler and shaker 2 mutants. The distributions of whirlin and myosin VIIa in stereocilia are mutually exclusive, with myosin VIIa tip localization being associated with impeded elongation of stereocilia.

strengths and weaknesses. Chimeric expression always requires de novo production by fusing mutant and wild-type components as embryos or ES cells. Mice mosaic for a null allele can be achieved by the partial somatic inactivation of targeted endogenous floxed alleles by the use of appropriate *Cre* transgenic mouse lines. Alternatively, Cre-mediated mitotic recombination techniques have the potential to simultaneously create a mosaic null and fluorescently label the genotype (53). Mosaic expression through the epigenetic process of female X inactivation has previously been used in conjunction with phenotypically neutral reporter genes to trace cell lineages during development (9, 45). In this report, we extend the use of female X-inactivation mosaicism to study gene function using a simple and reliable method. A mouse line can be established with the appropriate temporal-spatial expression for a given gene in approximately half of the normal complement of cells. We demonstrate that this method has particular utility in comparative analyses. The mosaic inner ear epithelia used in this study allow us to evaluate two cell populations side by side so that immunolabeling with specific antibodies and quantitative analyses of stereocilial dimensions can be performed with minimal measurement error with respect to the developmental differences between individual animals, variable conditions of sample preparation, and, most importantly, the changing morphology of hair bundles along the cochlear duct. In the apical turn, V-shaped bundles are formed by relatively few but generally long stereocilia, while in the basal turn, the bundles are W-shaped bundles and are composed of more numerous and shorter stereocilia. The transition between these two extremes is gradual, giving intermediate lengths and numbers of stereocilia in the middle turn, so careful measurements of the cochlear duct are necessary if one wants to compare corresponding hair cells in two different animals. The importance of mosaic analyses is accentuated further in mouse mutants exhibiting abnormally short cochlear ducts (e.g., looptail) (34).

In future applications, the mosaic analysis may be facilitated by using reporter genes linked to the BAC transgene or to the other *Hprt* allele, thus providing a cell-autonomous marker for visualizing which cells are complemented. Alternatively, the ability to monitor the expression, or deficiency, of the complementing protein may be achieved by fusion to fluorescent proteins or an antibody epitope tag. In this report, hair cell pathology itself was predictive of myosin VIIa deficiency, and reliable antibodies were available, so additional cell-autonomous markers were not essential for the mosaic analysis.

Mosaic complementation demonstrates that myosin VIIa is involved in the dynamic regulation of elongation of stereocilia. The lengths of stereocilia and the staircase-like organization of the bundle are critical to the sensitivity of hair cells. Each stereocilium is supported by a rigid paracrystalline array of tightly cross-linked, parallel actin filaments, which undergoes continuous turnover so that the length of a mature stereocilium is maintained in a dynamic steady state (39). However, the molecular factors involved in the dynamic regulation of elongation of stereocilia and postdevelopmental maintenance of their length gradation within the staircase are yet to be

defined. Here, we studied myosin VIIa, a positively oriented molecular motor expressed in hair cells that moves towards the plus ends of the actin filaments (49) at the stereocilial tips. The auditory sensory epithelium mosaic for myosin VIIa-deficient and -complemented hair cells demonstrated that stereocilia lacking myosin VIIa are longer than those of controls but shorten faster in the presence of an actin polymerization inhibitor. While our results obtained using cytochalasin D treatment disproved our working hypothesis that myosin VIIa has a role in promoting actin depolymerization at bases of stereocilia, they suggested the possibility of higher rates of actin polymerization in myosin VIIa-deficient stereocilia.

Our immunohistochemical analyses showed that both myosin XVa and whirlin, two proteins implicated in elongation of stereocilia (2, 3, 27, 40), localized to the tips of myosin VIIa-deficient stereocilia. However, myosin VIIa deficiency correlated with abnormally persistent whirlin localization in the tips of mature stereocilia of shorter rows, and this coincided with the higher intensity of whirlin-specific immunofluorescence in the hair cell cytoplasm. Most interestingly, we showed that myosin VIIa localized to the tips of the abnormally short stereocilia lacking whirlin or myosin XVa in *Whrn*$^{wi/wi}$ and *Myo15*$^{sh2/sh2}$ mice (32, 36). In wild-type mice, whirlin is detectable at the tips of all stereocilia during development but only at the tips of the most lateral (tallest) stereocilia in adults. Conversely, myosin VIIa is absent from tips of developing control stereocilia (our unpublished observations) while being present at the tips of shorter mature stereocilia. It is striking that the stereocilial distributions of whirlin and myosin VIIa are mutually exclusive. This negative correlation between the tip localizations of whirlin and myosin VIIa indicates the presence of an interacting protein(s) that either stops myosin VIIa from binding to the tip complex during development of stereocilia or promotes myosin VIIa binding at the tips of mature stereocilia.

The tips of stereocilia show morphological variations. The most lateral (tallest) stereocilia have dome-shaped tips filled with electron-dense material, while the pointed tips of stereocilia from shorter rows show only small electron-dense patches. The extent of electron density correlates with the levels of myosin XVa immunoreactivity at the tips of stereocilia (39). It is possible that the myosin XVa/whirlin complexes promote actin polymerization in proportion to their densities and that myosin VIIa competes with the scaffold proteins at the tips, thus regulating the speed of actin polymerization. The lack of myosin XVa or whirlin would allow myosin VIIa molecules between the plasma membrane and actin paracrystal, as we have observed in the abnormally short stereocilia of *Whrn*$^{wi/wi}$ and *Myo15*$^{sh2/sh2}$ mutant mice. Conversely, myosin VIIa deficiency would permit more whirlin molecules at the tips, resulting in abnormal elongation of stereocilia (Fig. 6). The lack of both whirlin and myosin VIIa would probably result in abnormally short stereocilia, as previously observed in shaker1/shaker2 double mutants (25), as the actin polymerization activity promoted by whirlin would be lost. The excessive elongation of myosin VIIa-deficient stereocilia would perturb the precision of their length gradation within a bundle, affecting the responses of hair cells to sound stimuli (44). Therefore, the dysregulation of the control of actin dynamics within stereocilia normally mediated by myosin VIIa is likely to be a major factor in the pathology of shaker1 in mice and Usher 1B in humans.

ACKNOWLEDGMENTS

We thank E. Grau and T. Hamilton for blastocyst injection; K. Wang, F. Law, and A. Beasley for technical assistance; T. B. Friedman for the kind gift of myosin XVa and whirlin antibodies; R. Gwilliam for human-specific primers; and K. Noben-Trauth for comments on the manuscript. FISH analysis was performed by R. Banerjee.

This work was supported by the Wellcome Trust, Medical Research Council, Deafness Research UK, and the European Commission (EuroHear LSHG-CT-2004-512063).

REFERENCES

1. **Araki, K., T. Imaizumi, K. Okuyama, Y. Oike, and K. Yamamura.** 1997. Efficiency of recombination by Cre transient expression in embryonic stem cells: comparison of various promoters. J. Biochem. (Tokyo) **122:**977–982.
2. **Belyantseva, I. A., E. T. Boger, and T. B. Friedman.** 2003. Myosin XVa localizes to the tips of inner ear sensory cell stereocilia and is essential for staircase formation of the hair bundle. Proc. Natl. Acad. Sci. USA **100:** 13958–13963.
3. **Belyantseva, I. A., E. T. Boger, S. Naz, G. I. Frolenkov, J. R. Sellers, Z. M. Ahmed, A. J. Griffith, and T. B. Friedman.** 2005. Myosin-XVa is required for tip localization of whirlin and differential elongation of hair-cell stereocilia. Nat. Cell Biol. **7:**148–156.
4. **Bronson, S. K., E. G. Plaehn, K. D. Kluckman, J. R. Hagaman, N. Maeda, and O. Smithies.** 1996. Single-copy transgenic mice with chosen-site integration. Proc. Natl. Acad. Sci. USA **93:**9067–9072.
5. **Call, L. M., C. S. Moore, G. Stetten, and J. D. Gearhart.** 2000. A cre-lox recombination system for the targeted integration of circular yeast artificial chromosomes into embryonic stem cells. Hum. Mol. Genet. **9:**1745–1751.
6. **Chada, K., J. Magram, K. Raphael, G. Radice, E. Lacy, and F. Costantini.** 1985. Specific expression of a foreign β-globin gene in erythroid cells of transgenic mice. Nature **314:**377–380.
7. **Chen, Y. T., and A. Bradley.** 2000. A new positive/negative selectable marker, *puΔtk*, for use in embryonic stem cells. Genesis **28:**31–35.
8. **Clark, A. J., G. Harold, and F. E. Yull.** 1997. Mammalian cDNA and prokaryotic reporter sequences silence adjacent transgenes in transgenic mice. Nucleic Acids Res. **25:**1009–1014.
9. **Collinson, J. M., R. E. Hill, and J. D. West.** 2004. Analysis of mouse eye development with chimeras and mosaics. Int. J. Dev. Biol. **48:**793–804.
10. **DeRosier, D. J., and L. G. Tilney.** 2000. F-actin bundles are derivatives of microvilli: what does this tell us about how bundles might form? J. Cell Biol. **148:**1–6.
11. **Ernest, S., G. J. Rauch, P. Haffter, R. Geisler, C. Petit, and T. Nicolson.** 2000. Mariner is defective in myosin VIIA: a zebrafish model for human hereditary deafness. Hum. Mol. Genet. **9:**2189–2196.
12. **Frengen, E., D. Weichenhan, B. Zhao, K. Osoegawa, M. van Geel, and P. J. de Jong.** 1999. A modular, positive selection bacterial artificial chromosome vector with multiple cloning sites. Genomics **58:**250–253.
13. **Gibson, F., J. Walsh, P. Mburu, A. Varela, K. A. Brown, M. Antonio, K. W. Beisel, K. P. Steel, and S. D. Brown.** 1995. A type VII myosin encoded by the mouse deafness gene shaker-1. Nature **374:**62–64.
14. **Guillot, P. V., L. Liu, J. A. Kuivenhoven, J. Guan, R. D. Rosenberg, and W. C. Aird.** 2000. Targeting of human eNOS promoter to the Hprt locus of mice leads to tissue-restricted transgene expression. Physiol. Genomics **2:**77–83.
15. **Hasson, T., M. B. Heintzelman, J. Santos-Sacchi, D. P. Corey, and M. S. Mooseker.** 1995. Expression in cochlea and retina of myosin VIIa, the gene product defective in Usher syndrome type 1B. Proc. Natl. Acad. Sci. USA **92:**9815–9819.
16. **Hasson, T., J. Walsh, J. Cable, M. S. Mooseker, S. D. Brown, and K. P. Steel.** 1997. Effects of shaker-1 mutations on myosin-VIIa protein and mRNA expression. Cell Motil. Cytoskel. **37:**127–138.
17. **Hasty, P., J. Rivera-Perez, C. Chang, and A. Bradley.** 1991. Target frequency and integration pattern for insertion and replacement vectors in embryonic stem cells. Mol. Cell. Biol. **11:**4509–4517.
18. **Heaney, J. D., A. N. Rettew, and S. K. Bronson.** 2004. Tissue-specific expression of a BAC transgene targeted to the *Hprt* locus in mouse embryonic stem cells. Genomics **83:**1072–1082.
19. **Hoess, R. H., A. Wierzbicki, and K. Abremski.** 1986. The role of the *loxP* spacer region in P1 site-specific recombination. Nucleic Acids Res. **14:**2287–2300.
20. **Holme, R. H., B. W. Kiernan, S. D. Brown, and K. P. Steel.** 2002. Elongation of hair cell stereocilia is defective in the mouse mutant whirler. J. Comp. Neurol. **450:**94–102.
21. **Holme, R. H., and K. P. Steel.** 2002. Stereocilia defects in waltzer (Cdh23), shaker1 (*Myo7a*) and double waltzer/shaker1 mutant mice. Hear. Res. **169:** 13–23.

22. **Hudspeth, A. J.** 1985. The cellular basis of hearing: the biophysics of hair cells. Science **230:**745–752.
23. **Hunter-Duvar, I. M.** 1978. A technique for preparation of cochlear specimens for assessment with the scanning electron microscope. Acta Otolaryngol. Suppl. **351:**3–23.
24. **Hurst, C. D., H. Fiegler, P. Carr, S. Williams, N. P. Carter, and M. A. Knowles.** 2004. High-resolution analysis of genomic copy number alterations in bladder cancer by microarray-based comparative genomic hybridization. Oncogene **23:**2250–2263.
25. **Karolyi, I. J., F. J. Probst, L. Beyer, H. Odeh, G. Dootz, K. B. Cha, D. M. Martin, K. B. Avraham, D. Kohrman, D. F. Dolan, Y. Raphael, and S. A. Camper.** 2003. *Myo15* function is distinct from *Myo6*, *Myo7a* and *pirouette* genes in development of cochlear stereocilia. Hum. Mol. Genet. **12:**2797–2805.
26. **Kiehart, D. P., J. D. Franke, M. K. Chee, R. A. Montague, T. L. Chen, J. Roote, and M. Ashburner.** 2004. Drosophila *crinkled*, mutations of which disrupt morphogenesis and cause lethality, encodes fly myosin VIIA. Genetics **168:**1337–1352.
27. **Kikkawa, Y., P. Mburu, S. Morse, R. Kominami, S. Townsend, and S. D. Brown.** 2005. Mutant analysis reveals whirlin as a dynamic organizer in the growing hair cell stereocilium. Hum. Mol. Genet. **14:**391–400.
28. **Kros, C. J., W. Marcotti, S. M. van Netten, T. J. Self, R. T. Libby, S. D. Brown, G. P. Richardson, and K. P. Steel.** 2002. Reduced climbing and increased slipping adaptation in cochlear hair cells of mice with *Myo7a* mutations. Nat. Neurosci. **5:**41–47.
29. **Lee, E. C., D. Yu, J. Martinez de Velasco, L. Tessarollo, D. A. Swing, D. L. Court, N. A. Jenkins, and N. G. Copeland.** 2001. A highly efficient Escherichia coli-based chromosome engineering system adapted for recombinogenic targeting and subcloning of BAC DNA. Genomics **73:**56–65.
30. **Liang, Y., A. Wang, I. A. Belyantseva, D. W. Anderson, F. J. Probst, T. D. Barber, W. Miller, J. W. Touchman, L. Jin, S. L. Sullivan, J. R. Sellers, S. A. Camper, R. V. Lloyd, B. Kachar, T. B. Friedman, and R. A. Fridell.** 1999. Characterization of the human and mouse unconventional *myosin XV* genes responsible for hereditary deafness DFNB3 and shaker 2. Genomics **61:**243–258.
31. **Liu, P., N. A. Jenkins, and N. G. Copeland.** 2003. A highly efficient recombineering-based method for generating conditional knockout mutations. Genome Res. **13:**476–484.
32. **Mburu, P., X. Z. Liu, J. Walsh, D. Saw, Jr., M. J. Cope, F. Gibson, J. Kendrick-Jones, K. P. Steel, and S. D. Brown.** 1997. Mutation analysis of the mouse *myosin VIIA* deafness gene. Genes Funct. **1:**191–203.
33. **Mburu, P., M. Mustapha, A. Varela, D. Weil, A. El-Amraoui, R. H. Holme, A. Rump, R. E. Hardisty, S. Blanchard, R. S. Coimbra, I. Perfettini, N. Parkinson, A. M. Mallon, P. Glenister, M. J. Rogers, A. J. Paige, L. Moir, J. Clay, A. Rosenthal, X. Z. Liu, G. Blanco, K. P. Steel, C. Petit, and S. D. Brown.** 2003. Defects in whirlin, a PDZ domain molecule involved in stereocilia elongation, cause deafness in the whirler mouse and families with DFNB31. Nat. Genet. **34:**421–428.
34. **Montcouquiol, M., R. A. Rachel, P. J. Lanford, N. G. Copeland, N. A. Jenkins, and M. W. Kelley.** 2003. Identification of *Vangl2* and *Scrb1* as planar polarity genes in mammals. Nature **423:**173–177.
35. **Nagy, A., and J. Rossant.** 2001. Chimaeras and mosaics for dissecting complex mutant phenotypes. Int. J. Dev. Biol. **45:**577–582.
36. **Probst, F. J., R. A. Fridell, Y. Raphael, T. L. Saunders, A. Wang, Y. Liang, R. J. Morell, J. W. Touchman, R. H. Lyons, K. Noben-Trauth, T. B. Friedman, and S. A. Camper.** 1998. Correction of deafness in *shaker-2* mice by an unconventional myosin in a BAC transgene. Science **280:**1444–1447.
37. **Ramirez-Solis, R., A. C. Davis, and A. Bradley.** 1993. Gene targeting in embryonic stem cells. Methods Enzymol. **225:**855–878.
38. **Roebroek, A. J., S. Reekmans, A. Lauwers, N. Feyaerts, L. Smeijers, and D. Hartmann.** 2006. Mutant *Lrp1* knock-in mice generated by recombinase-mediated cassette exchange reveal differential importance of the NPXY motifs in the intracellular domain of LRP1 for normal fetal development. Mol. Cell. Biol. **26:**605–616.
39. **Rzadzinska, A. K., M. E. Schneider, C. Davies, G. P. Riordan, and B. Kachar.** 2004. An actin molecular treadmill and myosins maintain stereocilia functional architecture and self-renewal. J. Cell Biol. **164:**887–897.
40. **Schneider, M. E., I. A. Belyantseva, R. B. Azevedo, and B. Kachar.** 2002. Rapid renewal of auditory hair bundles. Nature **418:**837–838.
41. **Self, T., M. Mahony, J. Fleming, J. Walsh, S. D. Brown, and K. P. Steel.** 1998. Shaker-1 mutations reveal roles for myosin VIIA in both development and function of cochlear hair cells. Development **125:**557–566.
42. **Slepecky, N. B., and Y. Ogata.** 1996. Immunohistochemical labeling of inner ear tissues embedded in polyethylene glycol 4000—comparative study with araldite and unicryl embedded sections. Nippon Jibiinkoka Gakkai Kaiho **99:**361–369.
43. **Soukharev, S., J. L. Miller, and B. Sauer.** 1999. Segmental genomic replacement in embryonic stem cells by double *lox* targeting. Nucleic Acids Res. **27:**e21.
44. **Stepanyan, R., I. A. Belyantseva, A. J. Griffith, T. B. Friedman, and G. I. Frolenkov.** 2006. Auditory mechanotransduction in the absence of functional myosin-XVa. J. Physiol. **576:**801–808.
45. **Stone, L. M., S. S. Tan, P. P. Tam, and T. E. Finger.** 2002. Analysis of cell lineage relationships in taste buds. J. Neurosci. **22:**4522–4529.
46. **Tam, P. P., and J. Rossant.** 2003. Mouse embryonic chimeras: tools for studying mammalian development. Development **130:**6155–6163.
47. **Todi, S. V., J. D. Franke, D. P. Kiehart, and D. F. Eberl.** 2005. Myosin VIIA defects, which underlie the Usher 1B syndrome in humans, lead to deafness in Drosophila. Curr. Biol. **15:**862–868.
48. **Toledo, F., C. W. Liu, C. J. Lee, and G. M. Wahl.** 2006. RMCE-ASAP: a gene targeting method for ES and somatic cells to accelerate phenotype analyses. Nucleic Acids Res. **34:**e92.
49. **Udovichenko, I. P., D. Gibbs, and D. S. Williams.** 2002. Actin-based motor properties of native myosin VIIa. J. Cell Sci. **115:**445–450.
50. **Wallace, H. A., F. Marques-Kranc, M. Richardson, F. Luna-Crespo, J. A. Sharpe, J. Hughes, W. G. Wood, D. R. Higgs, and A. J. Smith.** 2007. Manipulating the mouse genome to engineer precise functional syntenic replacements with human sequence. Cell **128:**197–209.
51. **Weil, D., S. Blanchard, J. Kaplan, P. Guilford, F. Gibson, J. Walsh, P. Mburu, A. Varela, J. Levilliers, M. D. Weston, et al.** 1995. Defective myosin VIIA gene responsible for Usher syndrome type 1B. Nature **374:**60–61.
52. **Zeng, C., N. Kouprina, B. Zhu, A. Cairo, M. Hoek, G. Cross, K. Osoegawa, V. Larionov, and P. de Jong.** 2001. Large-insert BAC/YAC libraries for selective reisolation of genomic regions by homologous recombination in yeast. Genomics **77:**27–34.
53. **Zong, H., J. S. Espinosa, H. H. Su, M. D. Muzumdar, and L. Luo.** 2005. Mosaic analysis with double markers in mice. Cell **121:**479–492.